Performance evaluation of dye-sensitized solar cells (DSSCs) based on metal-free thieno[3,2-*b*]indole dyes

Alexander S. Steparuk[1], Roman A. Irgashev[1,2,*] , Ekaterina F. Zhilina[1], Viktor V. Emets[3], Vitaly A. Grinberg[3], Ekaterina V. Krivogina[4], Ekaterina V. Belova[5], Petr I. Lazarenko[6], Gennady L. Rusinov[1,2], and Sergey A. Kozyukhin[4,7]

[1] *Postovsky Institute of Organic Synthesis, Ural Branch of the Russian Academy of Sciences, Ekaterinburg, Russia 620137*
[2] *Ural Federal University Named After the First President of Russia B. N. Yeltsin, Ekaterinburg, Russia 620002*
[3] *Frumkin Institute of Physical Chemistry and Electrochemistry of the Russian Academy of Sciences, Moscow, Russia 119071*
[4] *Kurnakov Institute of General and Inorganic Chemistry of the Russian Academy of Sciences, Moscow, Russia 119991*
[5] *Department of Chemistry, Moscow State University, Moscow, Russia 119991*
[6] *National Research University of Electronic Technology, Moscow, Zelenograd, Russia 124498*
[7] *Moscow Institute of Physics and Technology (National Research University), Dolgoprudny, Moscow Region, Russia 141701*

ABSTRACT

A series of thieno[3,2-*b*]indole-based dyes (**IS 1–10**) was readily synthesized in three steps from 2-(thien-2-yl)thieno[3,2-*b*]indole as the key precursor, and further applied as photosensitizers for dye-sensitized solar cells (DSSCs). In general, the prepared dyes have a push–pull (donor-π-linker-acceptor) structure, included thieno[3,2-*b*]indole ring system, bearing different aliphatic substituents at the nitrogen atom, as an electron-donating part, single thiophene unit as π-linker, and 2-cyanoacrylic acid (**IS 1–5**), or 5-(methylene)barbituric acid (**IS 6–10**) as an acceptor-anchoring group. The DSSC devices based on **IS 1–10** dyes were fabricated using commercially available TiO_2-coated photoanodes, and their photovoltaic characteristics were investigated. The DSSCs based on **IS 1–5** dyes exhibited values of power conversion efficiency (PCE) in the range of 2.25–3.02%, while the DSSCs based on **IS 6–10** dyes showed significantly low values of PCE in the range of 0.20–0.32% under AM 1.5G illumination (100 mW cm^{-2}). The highest PCE value of 3.02% (J_{sc} = 7.59 mA cm^{-2}, V_{oc} = 0.62 V, FF = 0.64) was achieved for DSSC based on dye **IS 4**, bearing 2-cyanoacrylic acid as an acceptor-anchoring group among all dyes **IS 1–10**, whereas **IS 9**, bearing 5-(methylene)barbituric acid displays best PCE of 0.32% (J_{sc} = 0.87 mA cm^{-2}, V_{oc} = 0.53 V and FF = 0.68) among dyes **IS 6–10**. Therefore, additional studies, including thermogravimetric analysis, UV–Vis, and FTIR-measurements on the TiO_2 surface, cyclic voltammograms, and photoelectrochemical measurements, were carried out for these two dyes.

Address correspondence to E-mail: irgashev@ios.uran.ru

Springer

1 Introduction

In general, solar cells represent a large family of photovoltaic devices, which can be constructed on inorganic or organic semiconductor materials as well as their various combinations and utilize for the direct conversion of sunlight energy to electricity [1]. Among them, dye-sensitized solar cells (DSSCs), reported for the first time by Grätzel and co-workers in 1991 [2], are a class of low-cost solar energy-to-electrical power conversion devices, wherein roles of light absorption and charge carrier transport are separated between different components of their photoelectrochemical system [3]. Indeed, further, DSSC devices are a promising alternative to the conventional Si-based solar cells due to their easy fabrication process as well as wide opportunities for the modification of their components, e.g., dye sensitizer or electrolyte system, affording to improve their stability and power conversion efficiency (PCE) [4]. Thus, the elaboration and study of new sensitizers that are one of the key components of DSSC, have attracted a considerable attention of many researchers in recent years as an appropriate way to form high-performance DSSC devices [5–8]. In this field, Ru(II)-based complex compounds were initially suggested as the effective sensitizers for DSSCs [2, 3]. However, Ru(II)-based sensitizers are limited for practical use due to their expensive, difficulty in synthesis and purification, and toxicity both for humans and the environment [5]. In turn, metal-free organic dyes, typically having donor-π-linker-acceptor (D-π-A) structure, in DSSCs demonstrated PCE and fill factor values comparable with the ruthenium dyes [5, 7, 9]. Moreover, metal-free organic dyes have a number of advantages for DSSC applications, such as high molar extinction coefficients, tunable optical and electrochemical properties, low cost of their synthesis due to the use of easy to perform procedures, and inexpensive chemicals [10]. Therefore, metal-free sensitizers are of important objectives for organic synthesis, since their use in DSSCs is one of the perspective ways to develop devices with improved characteristics [7, 11, 12]. It should be noted that many π-conjugated organic compounds, containing thiophene and pyrrole rings in the structure, have been declared as effective materials for organic photovoltaics, including DSSCs [13–15]. Among them, metal-free dyes, bearing electron-rich

carbazole or thieno[3,2-*b*]indole (TI) ring system as a donor part in their push–pull structure, have been successfully applied in the construction of high-performance DSSC devices [16–18]. In this context, we have previously described an effective route for the synthesis of TI-based dyes **IS 1–4**, shown in Scheme 1 and their primary application as photosensitizers in DSSCs [19].

Herein, we wish to present the expanded series of dyes **IS**, containing two numbers of TI-based sensitizers, namely **IS 1–5** and **IS 6–10**, bearing 2-cyanoacrylic acid and 5-(methylene)barbituric acid as an acceptor-anchoring group, respectively (Scheme 1). In this work, we have studied for the first time the optical and electrochemical properties, adsorption ability of these dyes as well as their application for the manufacture of DSSCs using commercially available TiO_2-coated photoanodes.

2 Experimental section

The synthesis of dyes **IS** and common information on the analytical equipment and methods used are described in Supplementary Information.

3 Results and discussion

3.1 Thermal properties of dyes *IS 4* and *IS 9*

The thermal gravimetric analysis curves of the synthesized dyes **IS 4** and **IS 9** are shown in Fig. 1. It can be seen that the analyzed **IS 4** decomposes in three steps, in contrast to **IS 9**. At the first step at 210–300 °C, **IS 4** exhibits a weight loss of 7% which is attributed to the elimination of the -CO_2H fragment, because only CO_2 is present in the gas phase ($m/z = 44$, $[CO_2]^+$, $m/z = 12$, $[C]^+$).
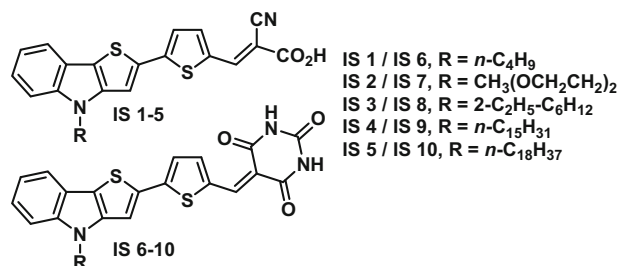
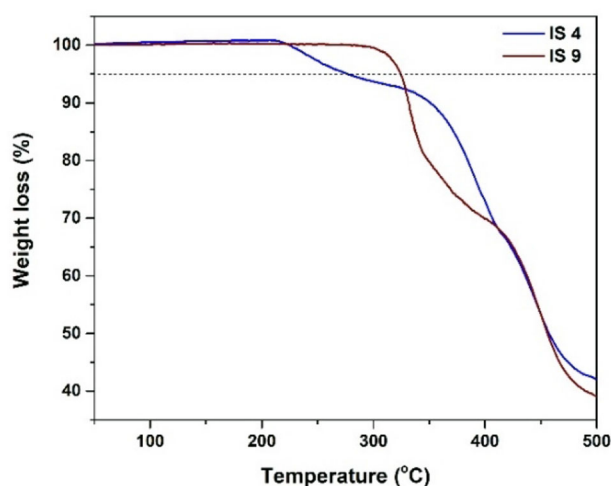

Scheme 1 The structure of TI-based dyes **IS 1–10**

Fig. 1 Thermogravimetric analysis of the dyes **IS 4** and **IS 9**

Further, decomposition occurs in two steps due to the loss of 26% at 300–410 °C and the loss of 27% at 410–500 °C, may be attributed to the decomposition of the dye molecule into fragments and their oxidation. The gaseous phase consisted mostly of corresponding products: $m/z = 78$, $[C_6H_6]+$, $m/z = 52$ $[C_4H_4]^+$ and $[C_3H_3N]^+$, $m/z = 26$, $[CN]+$, $m/z = 15$, $[CH_3]^+$, $m/z = 30$, $[C_2H_6]^+$, $m/z = 44$, $[CO_2]^+$, $m/z = 64$ $[SO_2]^+$, $m/z = 48$ $[SO]^+$, and $m/z = 18$ $[H_2O]^+$. A similar tendency was observed for **IS 9**.

Nonetheless, synthesized dyes **IS 4** and **IS 9** display relatively high decomposition temperatures of 276.6 °C and 324.5 °C in the air with 5% weight loss, respectively. These data show that the thermal stability of the obtained dyes is good enough for applications in DSSCs.

3.2 Optical and electronic properties of dyes *IS 1–10*

The absorption and normalized emission spectra of the dyes **IS 1–10** in CHCl₃ are shown in Fig. 2, the corresponding data are summarized in Table 1. The main part of the electronic absorption of these dyes **IS 1–10** carried out in the visible region at 400–610 nm, which is related to intramolecular charge transfer (πD-π*A) from the donor part of thieno[3,2-*b*]indole to the acceptor part of 2-cyanoacrylic acid or 5-(methylene)barbituric acid. The red shifts of the absorption and fluorescence maximum for 5-(methylene)barbituric dyes **IS 6–10** are approximately 56 nm in comparison to 2-cyanoacrylic dyes **IS 1–5**, respectively. A similar

situation was observed for carbazole-based D-π-A dyes [20]. Thus, it can be assumed that the electron-accepting ability of 5-(methylene)barbituric acid unit is stronger than that of 2-cyanoacrylic acid.

The spectra of the dyes **IS 4** and **IS 9** upon absorption on the surface of the TiO₂ film are shown in Fig. 3. Dye **IS 4** exhibits a hypsochromic shift of 9 nm in comparison to solution in CHCl₃, which can be attributed to the deprotonation of the carboxylic group in the acceptor-anchoring group of 2-cyanoacrylic acid [21]. On the other hand, the absorption of **IS 9** anchored on the TiO₂ film exhibits a bathochromic shift of 38 nm indicating that has a stronger tendency to form *J*-type aggregation [22, 23]. Despite the large values of the absorption maximum and extinction coefficient for the dyes **IS 6–10**, their photovoltaic performance did not show a significant improvement, as reported below.

3.3 Adsorption properties of organic dyes on TiO₂

To study the adsorption ability of the synthesized dyes on the TiO₂ surface, FTIR spectra were recorded for free dyes powder **IS 4** and **IS 9** and these dyes adsorbed TiO₂ nanoparticles (Fig. 4). The C≡N frequencies (2214 cm⁻¹) were not changed in the spectra-free dyes powder **IS 4** and adsorbed TiO₂. In this way, no interaction occurred between the C≡N moieties and TiO₂ during the adsorption. The O–H (3095 cm⁻¹) and C=O (1680 cm⁻¹) frequencies in the neat sample disappeared or shifted after dye adsorption, respectively. Therefore, the anchoring of **IS 4** dyes on the TiO₂ surface occurs through the carboxylate group and has the character of chemical adsorption. While bands for dye **IS 9** after adsorption were slightly shifted around 5–10 cm⁻¹, compared with the dye powder. This change can be assigned to the physical interactions on the TiO₂ surface.

3.4 Electrochemical properties of the dyes IS 4 and IS 9

The electrochemical properties of the dyes **IS 4** and **IS 9** were studied by cyclic voltammetry. The cyclic voltammograms are shown in Fig. 5, which demonstrate quasi-reversible oxidation and reduction processes for **IS 4** whereas **IS 9** exhibits quasi-reversible oxidation and electrochemically inactive in a wide range of cathodic potentials. On the base of the redox
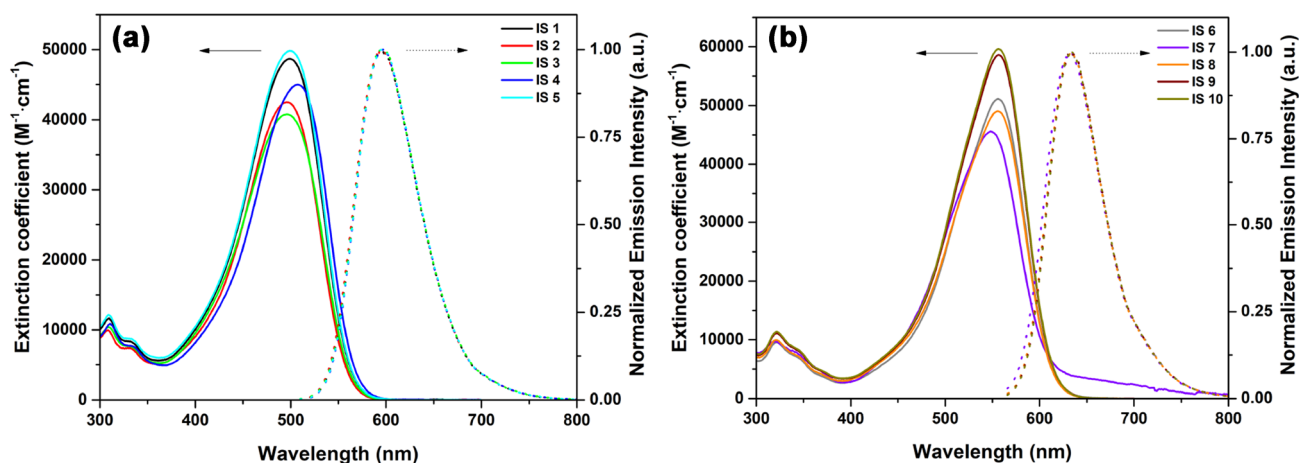
Fig. 2 a The absorption and normalized emission spectra of the dyes IS 1–5 and b IS 6–10

Table 1 Optical and electronic properties of IS 1–10

Dye	λ_{max} (nm)[a]	ε (M^{-1} cm^{-1})[b]	λ_{em} (nm)[c]	E_{0-0} (eV)[d]
IS 1	499	49,000	594	2.25
IS 2	496	42,700	597	2.27
IS 3	496	40,200	597	2.26
IS 4	506	45,000	596	2.25
IS 5	499	49,700	597	2.25
IS 6	556	51,100	633	2.07
IS 7	552	45,100	634	2.11
IS 8	556	48,100	633	2.07
IS 9	556	58,900	634	2.08
IS 10	556	59,600	634	2.06

[a]Absorption maximum in $CHCl_3$

[b]The molar extinction coefficient in $CHCl_3$

[c]Fluorescence emission maximum in $CHCl_3$

[d]The band gap E_{0-0} was derived from the intersecting point of absorption and normalized emission spectra in $CHCl_3$

Fig. 3 The normalized absorption spectra of the dyes IS 4 and IS 9 anchored on TiO_2 films

potentials dyes IS 4 and IS 9, HOMO and LUMO energy levels were calculated. The related data are listed in Table 2.

To estimate the feasibility of electron injection and regeneration processes, we performed the comparison of the dye's energy levels with those of the TiO_2 conduction band and redox electrolyte.

As shown in Fig. 6, the HOMO energy levels of dyes IS 4 and IS 9 are located lower than the potential of I^-/I_3^- redox couple (− 4.9 eV), which provides possible regeneration of oxidized dye molecules after injection of excited electrons into TiO_2 electrode. In turn, the latter process is energetically
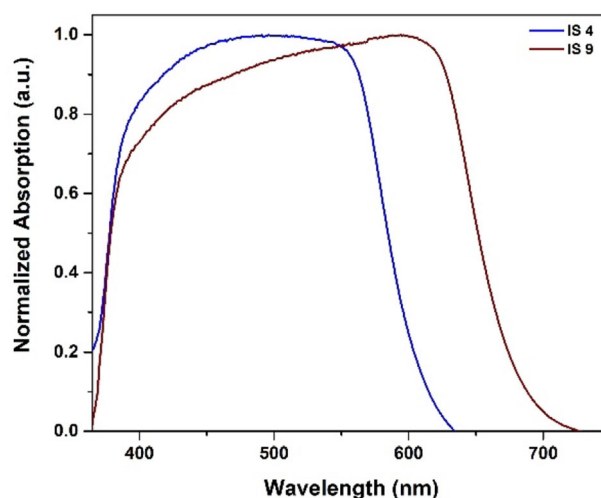
permitted for each of these dyes because their LUMO energy levels are located higher than the conduction edge of the TiO_2 (− 3.9 eV). Thus, dyes IS 4 and IS 9 are potentially appropriate as photosensitizers for DSSCs.

3.5 Photoelectrochemical characteristic of TiO_2-based photoanodes with dyes IS 1–5 and IS 9

To compare the photoelectrochemical properties of TiO_2-based photoanodes sensitized with dyes IS 1–5 and IS 9, we used a 3-electrode PECC-2 cell, which provides the equal experimental conditions for the photoelectrochemical test, and as a mediator, the standard system I^-/I_3^- (0.5 M LiI + 0.05 M I_2) in
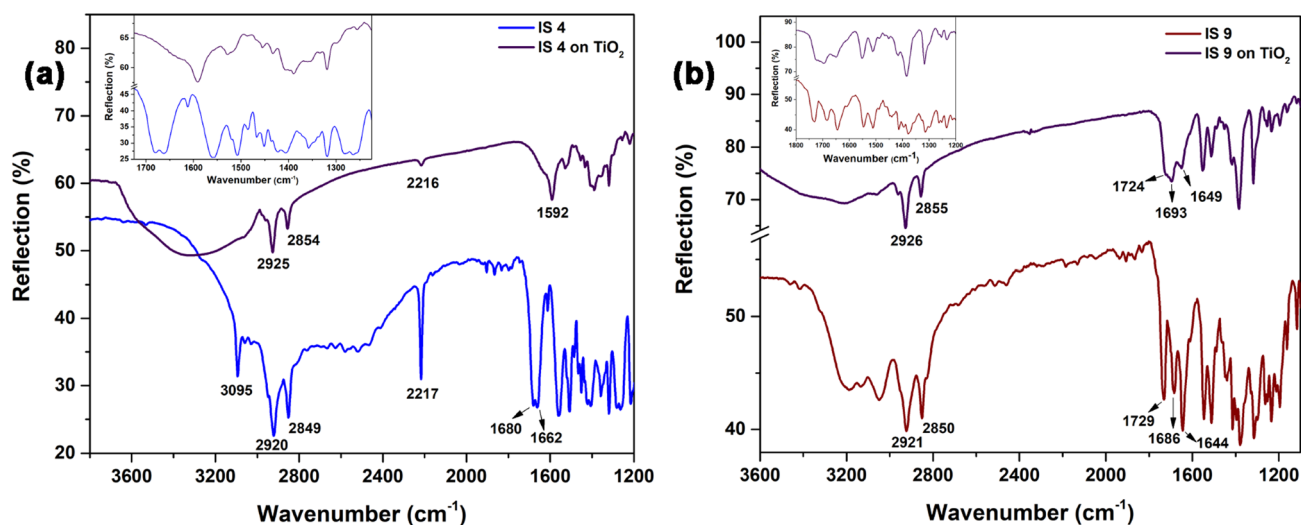
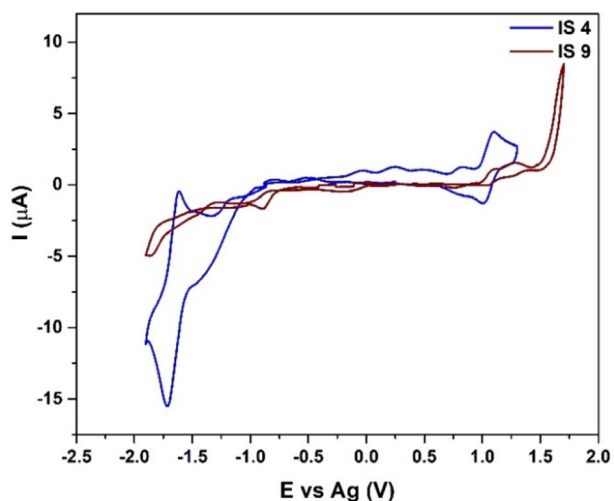Fig. 4 FTIR spectra of dye **IS 4** and **IS 9** powder and dye **IS 4**, **IS 9** adsorbed on TiO$_2$ nanoparticles

Fig. 5 Cyclic voltammogram on **GC** electrode for **IS 4** and **IS 9**

Fig. 6 Schematic energy levels of dyes **IS 4** and **IS 9**, a nanocrystalline TiO$_2$ electrode, and I_3^-/I^- redox electrolyte

Table 2 Electrochemical properties of the **IS 4** and **IS 9** dyes

Dye	E_{Ox}^{onset} (V)	E_{Red}^{onset} (V)	E_{HOMO} (eV)[a]	E_{LUMO} (eV)
IS 4	0.96	− 1.04	− 5.62	− 3.62[b]
IS 9	0.99	–	− 5.65	− 3.57[c]

[a]$E_{HOMO} = − [E_{ox}^{onset} − E_{1/2}(F_c/F_c^+) + 4.8]$, where $E_{1/2}(F_c/F_c^+)$ is the half-wave potential of the F_c/F_c^+ couple against the Ag electrode. It was defined at 0.14 V in the calibration experiment

[b]$E_{LUMO} = − [E_{red}^{onset} − E_{1/2}(F_c/F_c^+) + 4.8]$

[c]$E_{LUMO} = E_{0-0} + E_{HOMO}$

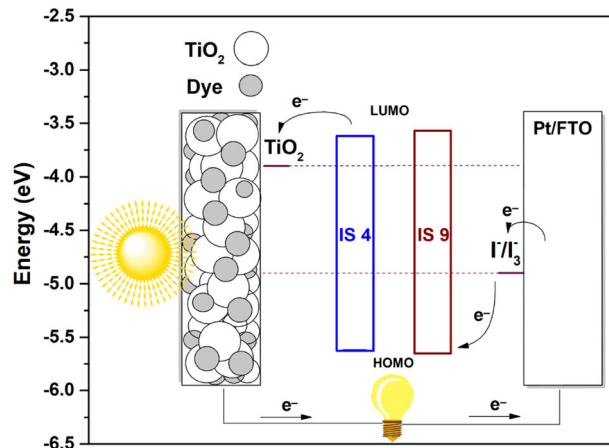acetonitrile. The structure of the **IS** dyes determines the efficiency of light absorption by molecules, their adsorption on the TiO$_2$ surface, and electron injection, and also affects the recombination losses and the efficiency of electron collection. The integral photoelectrochemical activity of photoanodes sensitized with dyes **IS 1–5** and **IS 9** was obtained under illumination with a solar spectrum simulator with a power of 100 mW cm^{-2} are shown in Fig. 7, the corresponding data are summarized in Table 3. It is noticeable that the photovoltaic parameters of TiO$_2$-based photoanodes sensitized with dyes depend on the nature of the acceptor-anchor part of the **IS** dyes. Dye **IS 4**, bearing 2-cyanoacrylic acid as an acceptor-anchoring group exhibits a PCE of 3.06% ($J_{sc} = 7.72$ mA cm^{-2}, $V_{oc} = 0.69$ V, and FF = 0.57), whereas **IS 9**, bearing 5-(methylene)barbituric acid

displays very low PCE of 0.58% (J_{sc} = 1.37 mA cm^{-2}, V_{oc} = 0.61 V and FF = 0.69), respectively.

The spectral dependences of the external quantum efficiency are shown in Fig. 8. It is obvious that the main spectral range of operation of photoanodes sensitized with dyes **IS 1–5** and **IS 9** falls within the wavelength range of 365–650 nm. The maximum values of IPCE for all photoanodes are observed in the range 450–470 nm. In the all-spectral range, the IPCE values for photoanodes based on **IS 1–5** sensitizers are 5–6 times higher than for **IS 9**. The IPCE data correspond to the main current–voltage characteristics. The IPCE spectrum is simultaneously influenced by several factors: light collection efficiency, electron injection, and carrier collection efficiency. In the case of **IS 1–5**, due to the presence of the 2-cyanoacrylic acid as acceptor-anchoring group, the dye molecules are reliably chemisorbed on the TiO$_2$ surface, which ensures a high surface concentration of dye molecules and efficient light absorption by the photoanode. Apparently, 5-(methylene)barbituric acid part of the molecule **IS 9** is not a sure anchoring group and cannot provide good adsorption of this dye on TiO$_2$ surface. As a result, dye molecules are bound to the TiO$_2$ surface only due to physical adsorption. This leads to a reduced concentration of dye **IS 9** per unit TiO$_2$ surface and, as a consequence, insufficiently effective light absorption by the photoanode. The presence of the 5-(methylene)barbituric acid acceptor-anchoring group in dye **IS 9** can also obstruct the injection of electrons.
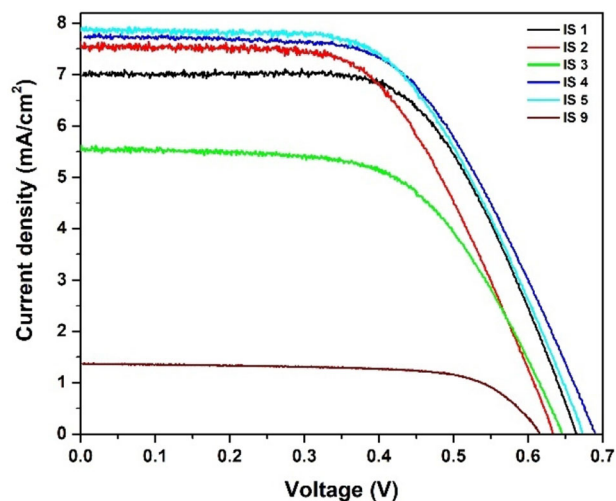
Table 3 Main photoelectrochemical characteristics of TiO$_2$-based photoanodes with dyes **IS 1–5** and **IS 9** with a mediator system 0.5 M LiI + 0.05 M I$_2$ in acetonitrile

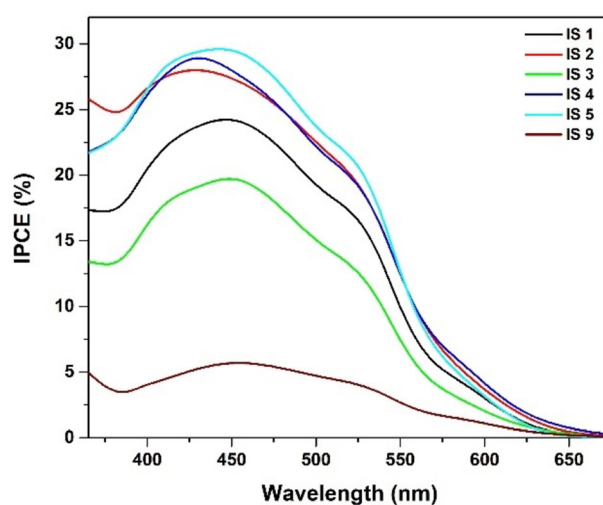| Dye	J_{sc} (mA cm^{-2})	V_{oc} (V)	FF	PCE (%)
IS 1	6.97	0.66	0.63	2.88
IS 2	7.64	0.63	0.57	2.75
IS 3	5.55	0.64	0.60	2.14
IS 4	7.72	0.69	0.57	3.06
IS 5	7.90	0.67	0.57	3.03
IS 9	1.37	0.61	0.69	0.58

Fig. 8 IPCE spectra of TiO$_2$-based photoanodes with dyes **IS 1–5** and **IS 9**

As noted, the anchoring function of the acceptor-anchoring groups in the thieno[3,2-*b*]indole dyes can affect the recombination and collection efficiency of electrons. This can be qualitatively judged by the transient of the photopotential. The transients of the photopotential for photoanodes **IS 4** and **IS 9** in the dark and under illumination with a 100 mW cm^{-2} solar simulator are shown in Fig. 9.

As can be seen from Fig. 9, under dark conditions, the potentials of the photoanodes are close. Under illumination with simulated sunlight, the potential of each photoanode quickly shifts to the cathode region. The cathodic shift increases on going from **IS 9** to **IS 4**. This is consistent with the corresponding increase in V_{oc} in Table 3. When the light is turned off, the potential of photoanodes **IS 4** relaxes more slowly to the dark potential as compared to **IS 9**. This indicates

Fig. 7 Photocurrent *vs* the voltage for the PECC of TiO$_2$-based photoanodes with dyes **IS 1–5** and **IS 9**

an increase in the lifetime of electrons going from **IS 9** to **IS 4**.

The recombination losses and the collection efficiency of electrons were quantified by modulation photocurrent spectroscopy (IMPS) and photovoltage spectroscopy (IMVS). The IMPS and IMVS spectra obtained under illumination with monochromatic light (λ = 453 nm, which coincides with the maximum value of IPCE) are shown in Figs. 10 and 11. It can be seen that the real component of the IMPS spectrum is higher for **IS 1–5** and significantly decreases on going to **IS 9**, which is consistent with the corresponding characteristics of short-circuit photocurrent density.

The electron transfer time (τ_{tr}) was estimated from the IMPS spectra using the equation:

$$\tau_{tr} = \frac{1}{2\pi f_{tr}}, \tag{1}$$

where f_{tr} is the characteristic minimum of the frequency of the imaginary component of the IMPS.

The electron lifetime (τ_{rec}) was estimated from the IMVS spectra using the equation:

$$\tau_{rec} = \frac{1}{2\pi f_{rec}}, \tag{2}$$

where f_{rec} is the minimum frequency of the imaginary component of the IMPS.

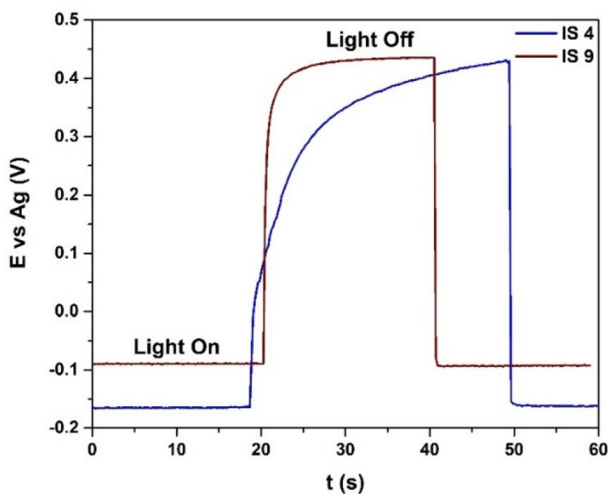The charge collection efficiency (η_{cc}) was determined by the equation:

Fig. 9 Time dependence of photoanode potential for PECC with photoanode based on sensitizers **IS 4** and **IS 9** adsorbed on titanium dioxide in the dark and on exposure to light of power 100 mW cm^{-2}
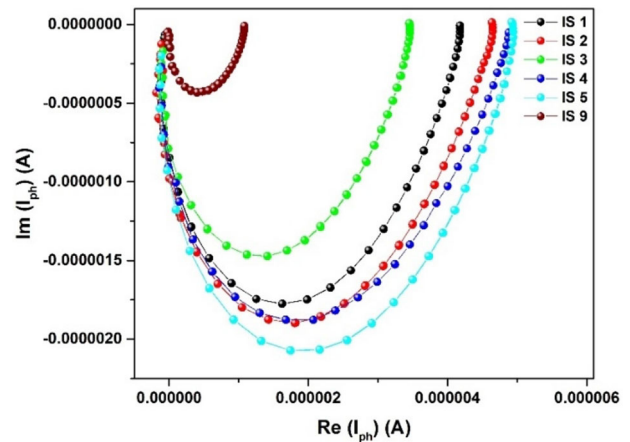
Fig. 10 Photocurrent spectra (IMPS) for PECC of TiO$_2$-based photoanodes with dyes **IS 1–5** and **IS 9**
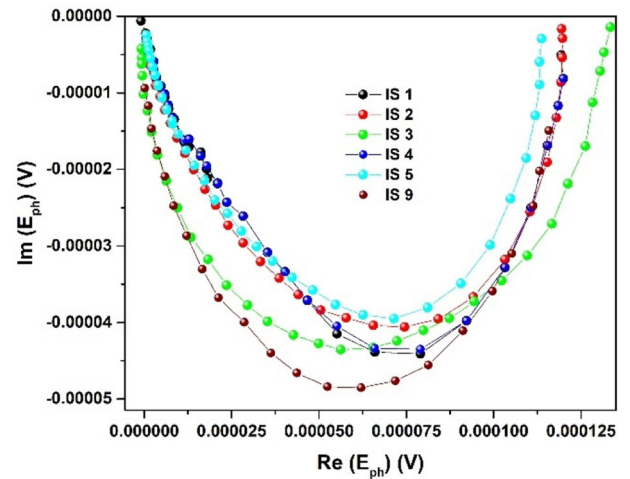
Fig. 11 Photopotential spectra (IMVS) for PECC of TiO$_2$-based photoanodes with dyes **IS 1–5** and **IS 9**

$$\eta_{cc} = 1 - \frac{\tau_{tr}}{\tau_{rec}}. \tag{3}$$

The obtained values τ_{tr}, τ_{rec}, and η_{cc} are given in Table 4. It is noticeable that the value of τ_{tr} slightly depends on the nature of the dye. The lifetimes of an electron largely depend on the nature of the dye and increase significantly on going from **IS 9** to **IS 1–5**. It is also seen from the table that the electron lifetimes in the case of **IS 1–5** are 20–30 times longer than the corresponding transit times, which provides an electron collection efficiency of about 95–97%. In the case of **IS 9**, the electron collection efficiency is 20% lower.

Table 4 Data from IMPS and IMVS spectra for of TiO_2-based photoanodes with dyes **IS 1–5** and **IS 9** with a mediator system 0.5 M LiI + 0.05 M I_2 in acetonitrile

Dye	τ_{tr} (ms)	τ_{rec} (ms)	h_{cc}
IS 1	0.42	14.0	0.97
IS 2	0.39	8.0	0.95
IS 3	0.61	8.0	0.92
IS 4	0.51	14.7	0.97
IS 5	0.38	8.2	0.95
IS 9	0.50	2.2	0.77

Taking into account that the thickness of the active TiO_2 layer (L) is 10–15 μm, the electron diffusion coefficient (D) was calculated using the equation:

$$D = \frac{L^2}{2.35 \cdot \tau_{tr}}. \tag{4}$$

The values of the electron diffusion coefficient obtained in this way were $(1/2) \cdot 10^{-5}$ cm^2 s^{-1}.

Knowing D and τ_{rec}, the effective electron diffusion length (L_d) was determined by equation:

$$L_d = \sqrt{D \cdot \tau_{rec}}. \tag{5}$$

The calculated L_d values for photoanodes based on **IS 1–5** dyes were 4–6 μm. Thus, the value of L_d is approximately half of the thickness of the active layer of photoanodes. This is additional evidence that, when photoanodes with sensitizers **IS 1–5** function, electrons can effectively collect on the electrode before they recombine.

3.6 Photovoltaic performance of DSSCs based on dyes IS 1–10

To test the performance of the dyes **IS 1–10** under realistic conditions, we have manufactured laboratory samples of DSSCs. The electrolyte used in photoelectrochemical measurements was replaced with a mixture of 3-propyl-1-methylimidazolium iodide (0.6 M), lithium iodide (0.1 M), iodine (0.05 M), and 4-(*tert*-butyl)pyridine (0.5 M) in 3-methoxypropionitrile. This modification was made since 3-methoxypropionitrile has a higher boiling point and less volatility than acetonitrile. Thus, it can be used in real-life DSSC operating conditions. Also, Ru(II)-based complex compound **N719** was used as the reference dye. The J/V characteristics obtained at

166 mV s^{-1} for all fabricated DSSCs are shown in Fig. 12. The photovoltaic results are summarized in Table 5.

The overall efficiencies of the DSSCs based on dyes **IS 1–5**, bearing 2-cyanoacrylic acid as an acceptor-anchoring group were superior to that of the device constructed using dyes **IS 6–10**, bearing 5-(methylene)barbituric acid as an acceptor-anchoring group, which is consistent with the results described above. Undoubtedly, the DSSC based on **IS 4** demonstrated the highest PCE of 3.02% among these dyes **IS 1–10** (J_{sc} = 7.59 mA cm^{-2}, V_{oc} = 0.62 V and FF = 0.64), reaching ∼ 60% of the standard cell based on **N719**.

One of the features for DSSCs is the different shapes of the J/V characteristics obtained in the forward and reverse modes of voltage variation [24]. This is a hysteresis phenomenon varying with scan direction, external bias, and sweep rate during the J/V measurements [25]. The hysteresis behaviors of DSSCs based on **IS 4** demonstrated by comparing the J/V curves of the forward and reverse scans are shown in Fig. 13.

The hysteresis index (HI) is used to quantitatively describe this phenomenon, in particular, to gage the severity degree of the gap between the forward and reverse J/V curves. In this work, HI was calculated accordingly equation [26]:

$$H_{index} = \frac{PCE_R - PCE_F}{PCE_R}, \tag{6}$$
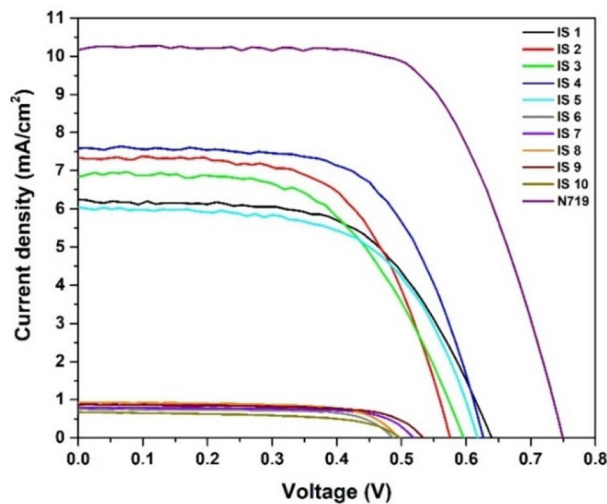

Fig. 12 J/V curves of DSSCs based on **IS 1–10** and **N719**

Table 5 Photovoltaic performance of the fabricated DSSCs based on **IS 1–10** and **N719**

Dye	J_{sc} (mA cm^{-2})	V_{oc} (V)	FF	PCE (%)
IS 1	6.24 ± 0.40	0.63 ± 0.01	0.60 ± 0.03	2.36 ± 0.29
IS 2	7.31 ± 0.40	0.57 ± 0.01	0.62 ± 0.04	2.59 ± 0.04
IS 3	6.89 ± 0.02	0.59 ± 0.01	0.58 ± 0.01	2.33 ± 0.05
IS 4	7.59 ± 0.13	0.62 ± 0.01	0.64 ± 0.01	3.02 ± 0.04
IS 5	6.02 ± 0.14	0.61 ± 0.01	0.61 ± 0.05	2.25 ± 0.25
IS 6	0.75 ± 0.01	0.48 ± 0.01	0.73 ± 0.02	0.26 ± 0.01
IS 7	0.79 ± 0.12	0.51 ± 0.01	0.73 ± 0.01	0.30 ± 0.01
IS 8	0.92 ± 0.03	0.49 ± 0.01	0.69 ± 0.08	0.31 ± 0.03
IS 9	0.87 ± 0.01	0.53 ± 0.01	0.68 ± 0.04	0.32 ± 0.02
IS 10	0.66 ± 0.02	0.49 ± 0.01	0.61 ± 0.02	0.20 ± 0.01
N719	10.22 ± 0.06	0.74 ± 0.01	0.66 ± 0.02	5.04 ± 0.21

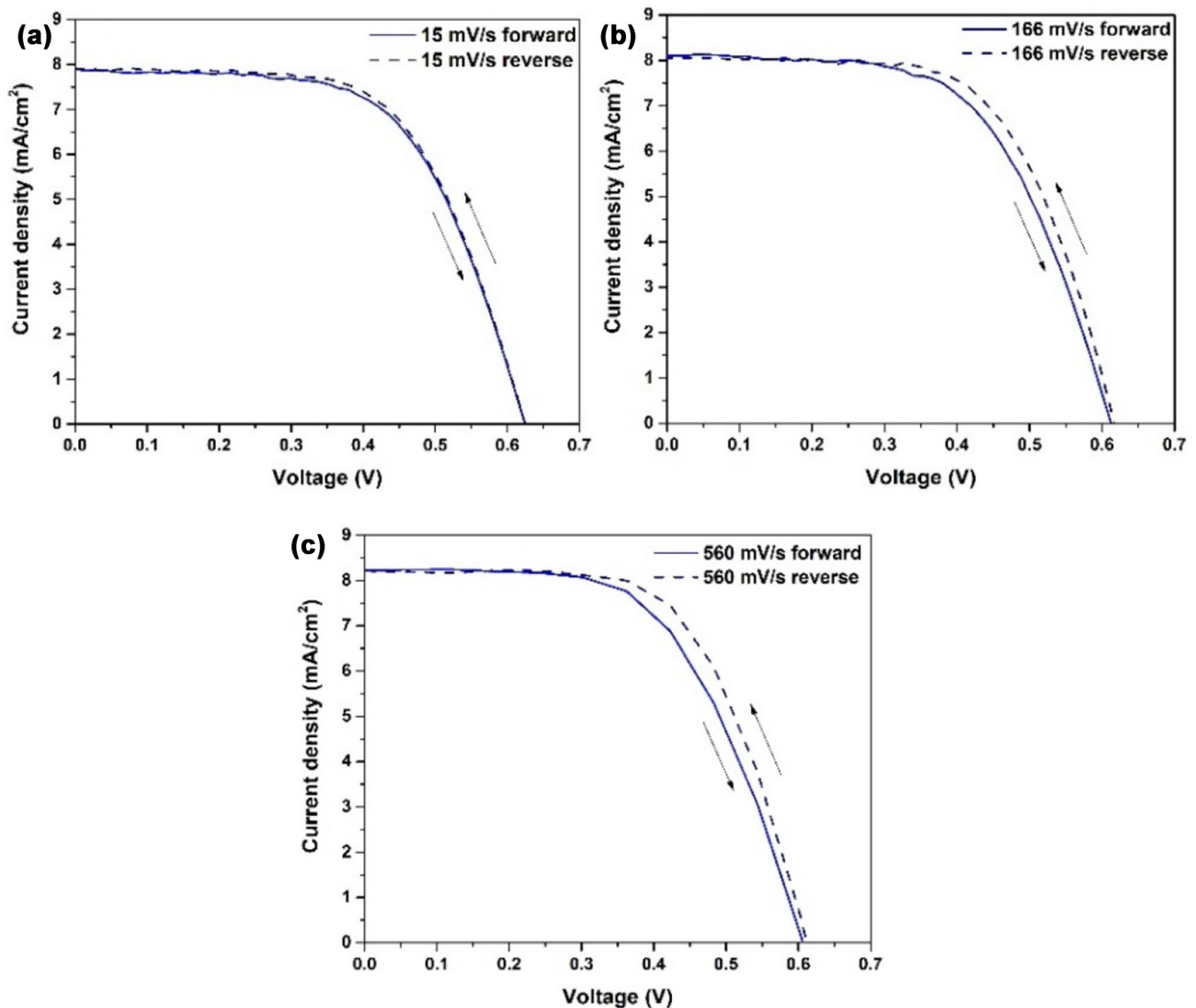The average performance parameters along with standard deviation errors for 3 parallel devices

Fig. 13 Reverse and forward scan *J/V* curves for best performing DSSCs based on **IS 4** with **a** 15, **b** 166, and **c** 560 mV s^{-1}

Table 6 Hysteresis index for DSSC based on **IS 4**

Scan rate (mV s^{-1})	Scan direction	J_{sc} (mA cm^{-2})	V_{oc} (V)	FF	PCE (%)	H_{index} (a.u.)
15	Forward	7.86	0.62	0.62	3.00	0.020
	Reverse	7.90	0.62	0.63	3.06	
166	Forward	8.11	0.61	0.59	2.91	0.064
	Reverse	8.05	0.61	0.63	3.11	
560	Forward	8.22	0.61	0.58	2.90	0.079
	Reverse	8.17	0.61	0.64	3.15	

where PCE_R and PCE_F are PCE obtained from the reverse and forward scanning directions, respectively.

The photovoltaic parameters including the calculated hysteresis index obtained for different scan rates are listed in Table 6. The photocurrent, FF, and PCE of investigated DSSCs for the forward scan are being higher than those from the reverse scan. So, the hysteresis index has a positive value for all measurements, which allows it to be identified as normal hysteresis [26].

Also, it should be noted that HI increases with increasing scan rate, which is typical for these devices [27, 28] as opposed to planar hybrid perovskite solar cells [29]. The change in hysteresis with these external test conditions might be related to multiple factors such as the electric field, electron diffusion, cell structure, and moreover. The mechanisms of the hysteresis phenomena have been described in several works [25, 27, 28] and not considered here. However, we suppose that the main reason of hysteresis obtained for these cells has been attributed to the presence of capacitance in the electrode–TiO$_2$–dye–electrolyte–electrode structure and the charge accumulation that are indirectly confirmed by the results of our previous study [30]. Reducing hysteresis leads to improving the overall photovoltaic performance of DSSCs. However, the capacitive elements cannot be fully removed as they are inherent properties of the corresponding components of DSSCs.

4 Conclusions

In summary, we have successfully prepared a wide series of metal-free D-π-A dyes (**IS 1–10**), bearing thieno[3,2-b]indole core as an electron-donating part and 2-cyanoacrylic acid (**IS 1–5**) and 5-(methylene)barbituric acid (**IS 6–10**) as electron acceptor-anchoring part and used these dyes as photosensitizers for DSSCs. In regard to the basic optical characteristics of the obtained dyes, **IS 6–10** showed generally higher extinction coefficients compared to **IS 1–5**. In addition, the absorption maxima of dyes **IS 6–10** were red shifted in comparison to the absorption maxima of dyes **IS 1–5**. Nevertheless, DSSCs based on dyes **IS 6–10** exhibited low PCE values at 0.20–0.32%, probably due to the poor binding ability of 5-(methylene)barbituric acid group in the structure of dyes **IS 6–10** to the TiO$_2$ surface, which caused to decrease overall sensitization activity of these dyes. In contrast to this, DSSCs based on dyes **IS 1–5**, bearing 2-cyanoacrylic acid as an anchoring group, showed PCE values at 2.25–3.02%. However, taking into account optical characteristics of dyes **IS 6–10**, further modification of their structure by addition of the functional substituents, bearing good anchoring function, e.g., –CO$_2$H group, at acceptor part of 5-(methylene)barbituric acid, can be a promising way to obtain photosensitizers with the improved properties.

Author contributions

Conceptualization: VVE, VAG, GLR, and SAK; device fabrication: ASS and EVK; methodology: ASS and RAI; validation: EFZ, EVB, and PIL; writing—original draft preparation: ASS and RAI; writing—review and editing: RAI and PIL; supervision: GLR and SAK.

Data availability

Supplementary data to this article can be found online at https://doi.org/10.1007/s10854-022-07805-w.

Code availability

Not applicable.

Declarations

Conflict of interest There are no conflicts to declare.

Supplementary Information: The online version contains supplementary material available at https://doi.org/10.1007/s10854-022-07805-w.

References

1. L. Fraas, L. Partain (eds.), *Solar Cells and Their Applications*, 2nd edn. (Wiley, Chichester, 2010)
2. B. O'Regan, M. Grätzel, Nature **353**, 737 (1991)
3. M. Grätzel, J. Photochem. Photobiol. C Photochem. Rev. **4**, 145 (2003)
4. A. Błaszczyk, in *Chem. Solut. Synth. Mater. Des. Thin Film Device Appl.* (Elsevier, 2021), pp. 509–544
5. C.P. Lee, C.T. Li, K.C. Ho, Mater. Today **20**, 267 (2017)
6. K. Sharma, V. Sharma, S.S. Sharma, Nanoscale Res. Lett. **13**, 1 (2018)
7. G. Boschloo, Front. Chem. **7**, 77 (2019)
8. H.A. Maddah, V. Berry, S.K. Behura, Renew. Sustain. Energy Rev. **121**, 109–678 (2020)
9. Z. Yao, M. Zhang, H. Wu, L. Yang, R. Li, P. Wang, J. Am. Chem. Soc. **137**, 3799 (2015)
10. N. Órdenes-Aenishanslins, G. Anziani-Ostuni, M. Vargas-Reyes, J. Alarcón, A. Tello, J.M. Pérez-Donoso, J. Photochem. Photobiol. B Biol. **162**, 707 (2016)
11. H. Jiang, Y. Wu, A. Islam, M. Wu, W. Zhang, C. Shen, H. Zhang, E. Li, H. Tian, W.H. Zhu, ACS Appl. Mater. Interfaces **10**, 13635 (2018)
12. Y. Mu, H. Wu, G. Dong, Z. Shen, S. Li, M. Zhang, J. Mater. Chem. A **6**, 21493 (2018)
13. P. Kumaresan, S. Vegiraju, Y. Ezhumalai, S. Yau, C. Kim, W.-H. Lee, M.-C. Chen, P. Kumaresan, S. Vegiraju, Y. Ezhumalai, S.L. Yau, C. Kim, W.-H. Lee, M.-C. Chen, Polymers (Basel). **6**, 2645 (2014)
14. S. Chaurasia, J.T. Lin, Chem. Rec. **16**, 1311 (2016)
15. Y. Li (ed.), *Organic Optoelectronic Materials* (Springer, Cham, 2015)
16. M. Liang, J. Chen, Chem. Soc. Rev. **42**, 3453 (2013)
17. Y. Wu, W. Zhu, Chem. Soc. Rev. **42**, 2039 (2013)
18. T.N. Murakami, N. Koumura, Adv. Energy Mater. **9**, 1802967 (2019)
19. A.S. Steparuk, R.A. Irgashev, G.L. Rusinov, E.V. Krivogina, P.I. Lazarenko, S.A. Kozyukhin, Russ. Chem. Bull. **68**, 1208 (2019)
20. R.A. Irgashev, G.A. Kim, G.L. Rusinov, V.N. Charushin, ARKIVOC **2014**, 123 (2014)
21. X.-H. Zhang, Y. Cui, R. Katoh, N. Koumura, K. Hara, J. Phys. Chem. C **114**, 18283 (2010)
22. R. Kesavan, F. Attia, R. Su, P. Anees, A. El-Shafei, A.V. Adhikari, J. Phys. Chem. C **123**, 24383 (2019)
23. L. Zhang, J.M. Cole, J. Mater. Chem. A **5**, 19541 (2017)
24. X. Yang, M. Yanagida, L. Han, Energy Environ. Sci. **6**, 54 (2012)
25. F. Wu, X. Li, Y. Tong, T. Zhang, J. Power Sources **342**, 704 (2017)
26. P. Liu, W. Wang, S. Liu, H. Yang, Z. Shao, Adv. Energy Mater. **9**, 1803017 (2019)
27. S. Sarker, H.W. Seo, Y.K. Jin, K.S. Lee, M. Lee, D.M. Kim, Electrochim. Acta **182**, 493 (2015)
28. H. Elbohy, H. El-Mahalawy, N.A. El-Ghamaz, H. Zidan, Electrochim. Acta **319**, 110 (2019)
29. H.J. Snaith, A. Abate, J.M. Ball, G.E. Eperon, T. Leijtens, N.K. Noel, S.D. Stranks, J.T.-W. Wang, K. Wojciechowski, W. Zhang, J. Phys. Chem. Lett. **5**, 1511 (2014)
30. P.I. Lazarenko, S.A. Kozyukhin, A.I. Mokshina, A.A. Sherchenkov, T.N. Patrusheva, R.A. Irgashev, E.A. Lebedev, V.V. Kozik, Russ. Phys. J. **61**, 196 (2018)

Publisher's Note Springer Nature remains neutral with regard to jurisdictional claims in published maps and institutional affiliations.